Journal of Power Sources 210 (2012) 96–100

Contents lists available at SciVerse ScienceDirect

Journal of Power Sources

journal homepage: www.elsevier.com/locate/jpowsour

Short communication

Electrical properties of the $GdSmZr_2O_7$ ceramic under different sintering conditions

Zhan-Guo Liu[a,b,c], Jia-Hu Ouyang[a,*], Ke-Ning Sun[b,c], Yu Zhou[a]

[a] Institute for Advanced Ceramics, School of Materials Science and Engineering, Harbin Institute of Technology, 92 West Da-Zhi Street, Harbin 150001, China
[b] Natural Science Research Center, Academy of Fundamental and Interdisciplinary Sciences, Harbin Institute of Technology, 2 Yi-Kuang Street, Harbin 150080, China
[c] Department of Applied Chemistry, Harbin Institute of Technology, 92 West Da-Zhi Street, Harbin 150001, China

ARTICLE INFO

Article history:
Received 27 December 2011
Received in revised form 6 March 2012
Accepted 9 March 2012
Available online 21 March 2012

Keywords:
Rare-earth zirconate
Pyrochlore
Solid electrolyte
Impedance spectroscopy
Electrical conductivity

ABSTRACT

The $GdSmZr_2O_7$ ceramic is prepared by pressureless-sintered method under different conditions as a possible solid electrolyte. The crystal structure, microstructure and electrical properties are characterized by the X-ray diffraction, field-emission scanning electron microscopy and ac impedance spectroscopy, respectively. The $GdSmZr_2O_7$ ceramic exhibits a single phase of the pyrochlore-type structure. The total conductivity of the $GdSmZr_2O_7$ ceramic obeys the Arrhenius relation, and gradually increases with increasing temperature from 723 to 1173 K. The $GdSmZr_2O_7$ ceramic is an oxide-ion conductor in the oxygen partial pressure range of 1.0×10^{-4} to 1.0 atm at all test temperature levels. According to the experimental results of the present work, the maximum value of the total conductivity for the $GdSmZr_2O_7$ ceramic is about 1.01×10^{-2} S cm^{-1} at 1173 K.

1. Introduction

Solid oxide electrolytes with high oxygen ion conductivity are of considerable interest for potential application in solid oxide fuel cells (SOFCs), oxygen pumps, oxygen sensors, and so on [1–3]. In the conventional SOFCs system, the electrolyte material is 8 mol.% yttria-stabilized zirconia (YSZ), and the anode material is Ni–YSZ cermet, and the cathode material is strontium-substituted manganites ($La_{1-x}Sr_xMnO_3$), respectively [4–6]. However, high operation temperatures promote unwanted reactions at the cathode/electrolyte interface, forming $La_2Zr_2O_7$ and $SrZrO_3$ resistive layers [7–9]. Both zirconate phases lead to a decrease in the electrical conductivity, and have greatly damage on the performance of SOFCs. The $A_2Zr_2O_7$-type (A = lanthanide) oxides have a pyrochlore-type structure or a defect fluorite-type structure, and exhibit the well-known ability of the structure to accommodate oxygen nonstoichiometry [10]. The electrical conductivity of the $Sm_2Zr_2O_7$ was comparable to those of other oxide-ion conductors in the low-temperature regions [11]. The electrical conductivity of $A_2Zr_2O_7$-type compounds can be improved by doping with different metal elements [8,12,13]. $Sm_2Zr_2O_7$ co-doped with 5 mol.% Gd and 5 mol.% Yb shows higher electrical conductivity than undoped $Sm_2Zr_2O_7$ in the temperature range of 723–1023 K [14]. It was found that the $GdSmZr_2O_7$ ceramic had the highest electrical conductivity in the $(Gd_{1-x}Sm_x)_2Zr_2O_7$ ($0 \le x \le 1.0$) system from 623 to 873 K [15].

It should be noted that sintering condition has a critical effect on the electrical conductivity of different solid oxide electrolytes. Sha et al. found that $Ce_{0.8}Sm_{0.1}Y_{0.1}O_{1.9}$ sintered at 1573 and 1673 K showed much higher total conductivity and lower activation energy than those sintered at 1773 and 1873 K [16]. Li et al. reported that Mg-doped $Gd_{0.1}Ce_{0.9}O_{1.95}$ sintered at 1573 K exhibited higher electrical conductivity than those sintered at 1373 and 1773 K, respectively [17]. In this work, the $GdSmZr_2O_7$ ceramic was prepared by pressureless-sintering method under different conditions, and the microstructure and electrical conductivity of the $GdSmZr_2O_7$ ceramic were investigated.

2. Experimental procedure

Polycrystalline $GdSmZr_2O_7$ ceramic were prepared via a solid state reaction route. Commercial powders of Gd_2O_3 (Rare-Chem Hi-Tech Co. Ltd., China; purity ≥ 99.99%), Sm_2O_3 (Rare-Chem Hi-Tech Co. Ltd., China; purity ≥ 99.99%), and ZrO_2 (Dongguan SG Ceramics Technology Co. Ltd., China; purity ≥ 99.9%) were weighed in the required stoichiometric ratio, and homogenized using zirconia balls and analytically pure alcohol. All oxide powders were calcined at 1173 K for 2 h in air prior to weighing. Green pellets were obtained by uniaxial pressing at 20 MPa and isostatic pressing at 200 MPa

* Corresponding author. Tel.: +86 451 86414291; fax: +86 451 86414291.
E-mail addresses: zgliu@hit.edu.cn (Z.-G. Liu), ouyangjh@hit.edu.cn (J.-H. Ouyang).

0378-7753/$ – see front matter © 2012 Elsevier B.V. All rights reserved.
doi:10.1016/j.jpowsour.2012.03.024

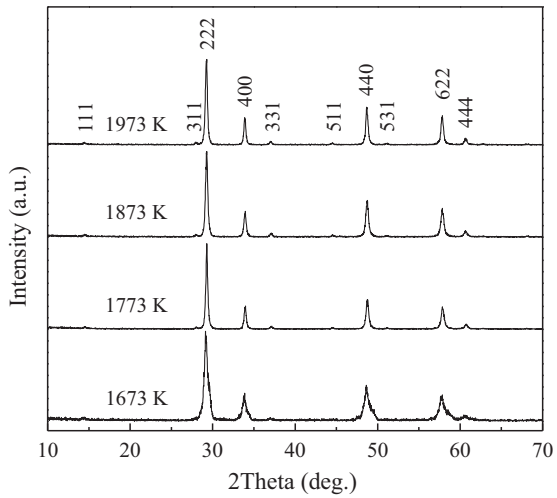

Fig. 1. XRD patterns of the $GdSmZr_2O_7$ ceramic sintered at different temperatures for 10 h in air.

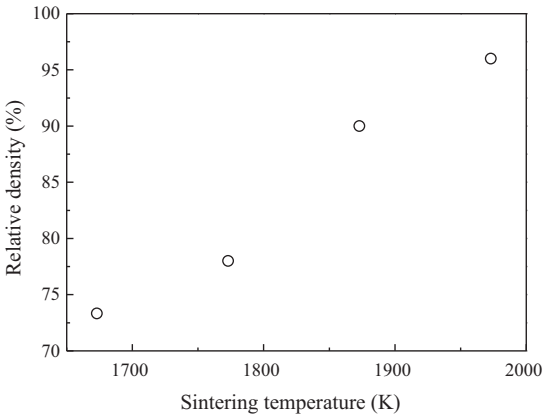

Fig. 2. Relative density of the $GdSmZr_2O_7$ ceramic sintered at different temperatures for 10 h in air.

for 5 min, and then sintered at different temperatures (1673, 1773, 1873 and 1973 K) for 10 h, respectively. All the pellets were sintered in air, and then furnace cooling to room temperature.

Phase identification and analysis of the sintered pellets were conducted by X-ray diffractometry (XRD). XRD data were collected on a diffractometer (Rigaku D/Max 2200VPC, Japan) using Cu Kα radiation at room temperature. A continuous scan mode was used to collect 2θ data from 10° to 70° in steps of 0.02° and a scanning rate of 5° min^{-1}. X-ray tube voltage and current were set at 40 kV and 30 mA, respectively. The bulk density of sintered pellets was determined by the usual volume and weight measurement technique. The as-sintered pellets were carbon coated for microstructural analysis using a field-emission scanning electron microscope (FEI Quanta 200F, the Netherlands).

AC impedance spectroscopy was carried out on sintered pellets using an impedance/gain-phase analyzer (Solartron^{TM} SI 1260, UK). Electrodes were prepared by coating both pellet faces with a platinum paste, and then heated at 1223 K for 2 h in air to decompose the paste and harden the Pt residue. Platinum wires were attached to the surface of the pellets for measurements. Measurements were performed in air between 723 and 1173 K, with a 20 mV signal amplitude at open circuit voltage in the 0.2 Hz to 2 MHz frequency range using the Zplot software. The impedance measurements as a function of oxygen partial pressure were performed in a closed

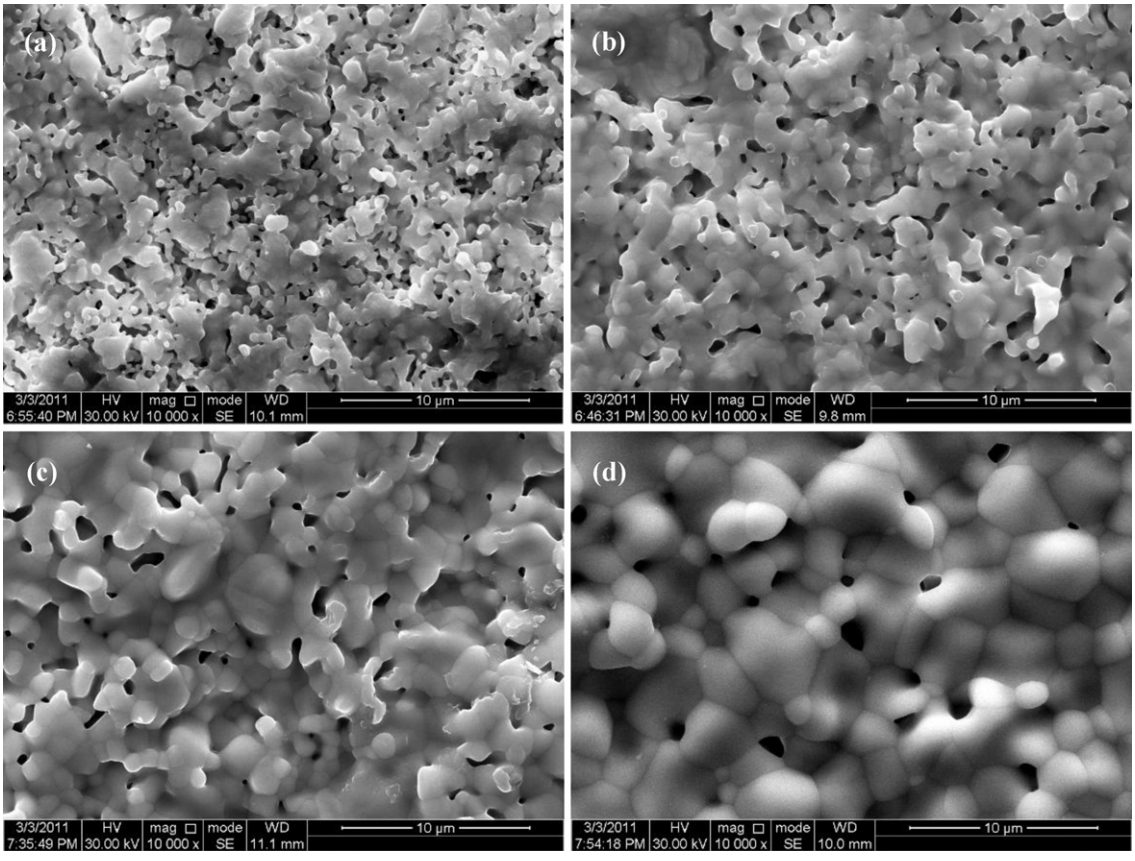

Fig. 3. Surface micrographs of the $GdSmZr_2O_7$ ceramic sintered at different temperatures for 10 h in air: (a) 1673 K, (b) 1773 K, (c) 1873 K, and (d) 1973 K.

tube furnace cell. The oxygen partial pressure $p(O_2)$ ranged from around 1.0×10^{-4} to 1.0 atm, and was monitored by an YSZ sensor. The process involved flushing the system with a N_2–O_2 gas mixture. All impedance data were analysed using Zview 3.1c software.

3. Results and discussion

Fig. 1 shows the results of the XRD analysis of the $GdSmZr_2O_7$ ceramic sintered at different temperatures for 10 h in air. It is clearly seen that XRD patterns of the $GdSmZr_2O_7$ ceramic sintered at 1773–1973 K in air are similar, however, the XRD pattern of the $GdSmZr_2O_7$ ceramic sintered at 1673 K exhibits wide diffraction peaks owing to lower sintering temperature. The $GdSmZr_2O_7$ ceramic crystallizes with a pyrochlore-type structure, which is characterized by the presence of typical super-lattice peaks at 2θ values of about 14° (1 1 1), 28° (3 1 1), 37° (3 3 1), 45° (5 1 1) and 51° (5 3 1) using Cu Kα radiation [18,19]. It indicates that the $GdSmZr_2O_7$ ceramic reacts to completion at 1673–1973 K for 10 h in air. Fig. 2 presents the variations in the relative density of the $GdSmZr_2O_7$ ceramic sintered at different temperatures for 10 h in air. Clearly, the relative density of the $GdSmZr_2O_7$ ceramic rapidly increases with increasing sintering temperature.

Typical surface micrographs of the $GdSmZr_2O_7$ ceramic sintered at different temperatures for 10 h in air are displayed in Fig. 3. From Fig. 3(a) and (b), there are many pores in the $GdSmZr_2O_7$ ceramic sintered at 1673–1773 K, as the relative density of the $GdSmZr_2O_7$ ceramic is less than 90%. With the increase of sintering temperature, different diffusion mechanisms such as grain boundary diffusion, bulk diffusion and surface diffusion contribute to densification during sintering. The pores become less and less, and the bulk ceramic becomes much denser, especially after sintering at 1973 K, which is consistent with the relative density. From Fig. 3(d), the grain size of the $GdSmZr_2O_7$ ceramic is 1–5 μm after sintering at 1973 K for 10 h in air.

Fig. 4(a)–(d) shows the impedance spectra taken at 723 K in air for the samples of the $GdSmZr_2O_7$ ceramic sintered at different temperatures. In the ideal case, the frequency response of the impedance of electroded polycrystalline electrolytes can be modeled by a resistor–capacitor (RC) pair in parallel. However, in the present case, in place of capacitor a constant phase element (CPE) is required to model the measured data [20]. According to the experimental data, and the following equivalent circuit was chosen for the fitting [20]: $(RC)_G(RC)_{GB}(RC)_E$, where the subscripts G and GB represent the grain and grain-boundary contributions, respectively, and E is the electrode processes, as shown in Fig. 4(e). The resistance in the high frequency range represents the grain resistance, and the resistance in the intermediate frequency range represents to the grain-boundary resistance. It clearly seen from Fig. 4 that the grain and grain-boundary resistance of the $GdSmZr_2O_7$ ceramic gradually decrease with increasing sintering temperature, and it means that the grain and grain-boundary conductivity of the $GdSmZr_2O_7$ ceramic gradually increase with increasing sintering temperature. However, it is not possible to accurately separate the total resistance (R) into the grain resistance and grain boundary resistance. Therefore, the intercept to the Z' axis of the intermediate frequency range is used to determine the total resistance ($R_G + R_{GB}$). The total conductivity of the $GdSmZr_2O_7$ ceramic sintered at different temperatures is determined from the values of the total resistance at the corresponding temperatures and the geometrical dimensions of the measured samples, respectively. In practice, the total conductivity may be more relevant compared to the grain or grain-boundary conductivity.

Fig. 5 shows the temperature dependent total conductivity of the $GdSmZr_2O_7$ ceramic sintered at different temperatures, which is obtained from 723 to 1173 K in air. The temperature dependence

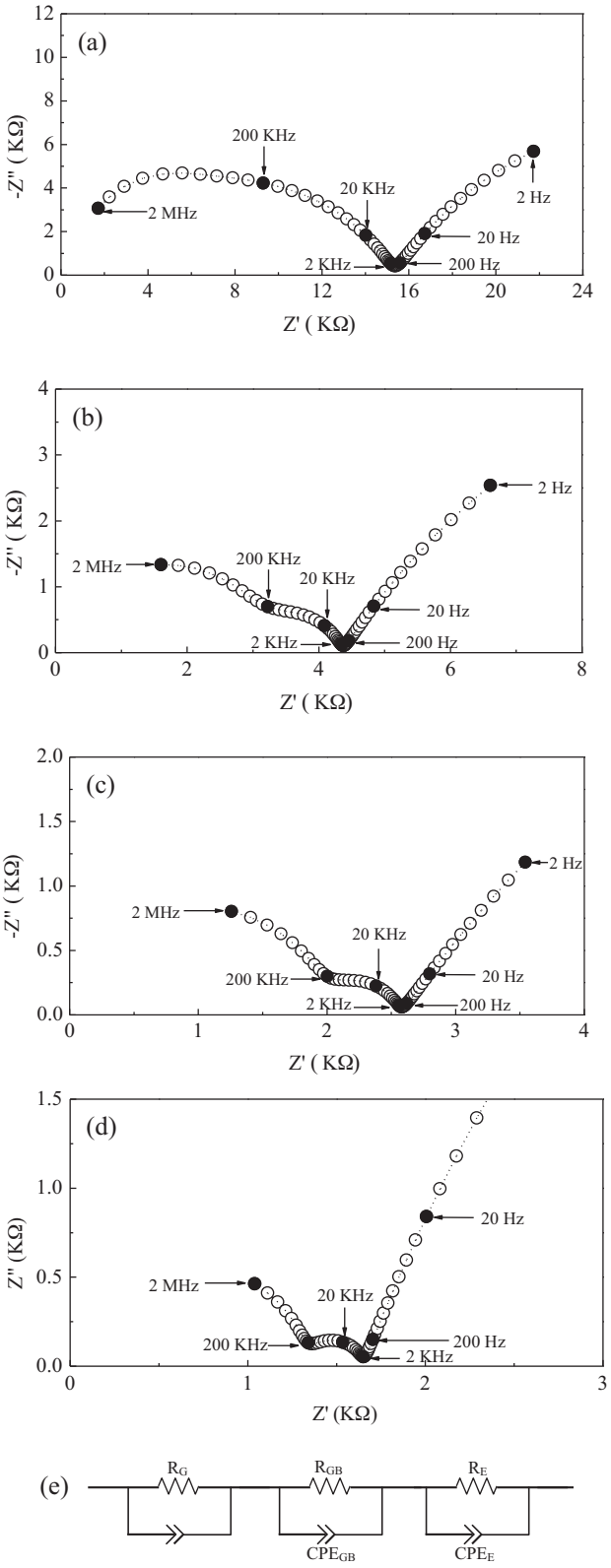

Fig. 4. Impedance spectra and schematic equivalent electrical circuit plots of the $GdSmZr_2O_7$ ceramic at 723 K in air: (a) sintered at 1673 K, (b) sintered at 1773 K, (c) sintered at 1873 K, (d) sintered at 1973 K, and (e) equivalent electrical circuit.

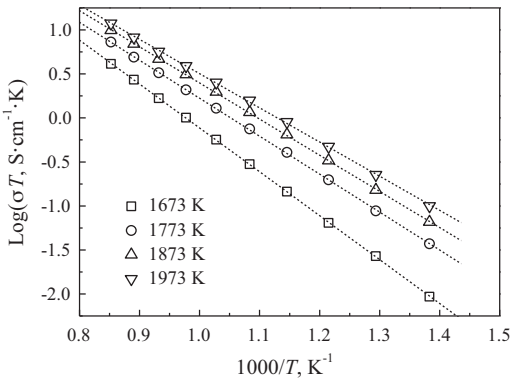

Fig. 5. Arrhenius plots of the total conductivity of the $GdSmZr_2O_7$ ceramic sintered at different temperatures.

of the total conductivity can be described by the Arrhenius equation,

$$\sigma \cdot T = \sigma_0 \exp\left(\frac{-E}{k_B T}\right) \quad (1)$$

where σ, T, σ_0, E and k_B are the total conductivity, absolute temperature, pre-exponential factor, activation energy and Boltzmann constant, respectively. It can be seen from Fig. 5 that the total conductivity of the $GdSmZr_2O_7$ ceramic follows the linear behavior, which indicates that the ionic diffusion process is thermally activated. It is evident that the total conductivity of the $GdSmZr_2O_7$ ceramic gradually increases with increasing temperature from 723 to 1173 K. From Fig. 5, the total conductivity of the $GdSmZr_2O_7$ ceramic gradually increases with increasing sintering temperature, which is caused by increasing relative density. The maximum value of the total conductivity for the $GdSmZr_2O_7$ ceramic is about 1.01×10^{-2} S cm^{-1} at the highest measured temperature of 1173 K and in air atmosphere. The total conductivities of other pyrochlore oxides, such as $Sm_2Zr_2O_7$ and $Nd_2Zr_2O_7$, are about 5.94×10^{-3} S cm^{-1} and 1.66×10^{-3} S cm^{-1} at 1173 K [21,22], respectively. It indicates that the total conductivity of the $GdSmZr_2O_7$ ceramic is obviously higher than those of $Sm_2Zr_2O_7$ and $Nd_2Zr_2O_7$. The activation energy and pre-exponential factor of the total conductivity for the $GdSmZr_2O_7$ ceramic are calculated from the slope and the intercept of the Arrhenius plots (Fig. 5), respectively. The calculated values of the activation energy and pre-exponential factor are shown in Fig. 6. It is clearly seen that the activation energy and pre-exponential factor of the total conductivity for the $GdSmZr_2O_7$ ceramic gradually decrease with increasing relative density. Using a simple adjustment of $1/(1 - \text{porosity})^2$ to correct the pre-exponential factors. The results are also shown in

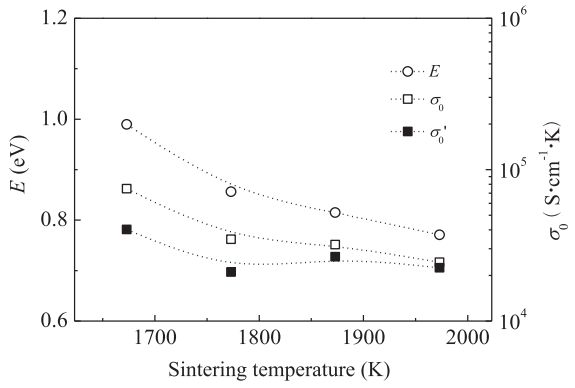

Fig. 6. Activation energy and pre-exponential factor for the total conductivity of the $GdSmZr_2O_7$ ceramic sintered at different temperatures.

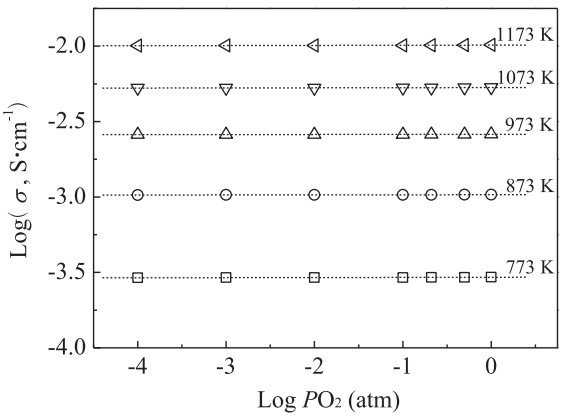

Fig. 7. Oxygen partial pressure dependence of the total conductivity of the $GdSmZr_2O_7$ ceramic sintered at 1973 K for 10 h in air.

Fig. 6, it can be seen that the corrected pre-exponential factors (σ_0') of the $GdSmZr_2O_7$ ceramic sintered at 1773–1973 K are approximately the same.

In order to clarify conduction carrier, the oxygen partial pressure $p(O_2)$ dependence of the total conductivity for the $GdSmZr_2O_7$ ceramic was measured. Fig. 7 shows the total conductivity of the $GdSmZr_2O_7$ ceramic sintered at 1973 K as a function of oxygen partial pressure at different temperatures. It can be seen that the total conductivity of the $GdSmZr_2O_7$ ceramic is almost independent of oxygen partial pressure from 1.0×10^{-4} to 1.0 atm at each test temperature, which indicates that the conduction of the $GdSmZr_2O_7$ ceramic is purely ionic conductivity with negligible electronic conduction [23]. The total conductivities of conventional solid oxide electrolytes such as $Zr_{0.92}Y_{0.08}O_{2-\delta}$, $Ce_{0.8}Gd_{0.2}O_{2-\delta}$, and $La_{0.80}Sr_{0.20}Ga_{0.76}Mg_{0.19}Co_{0.05}O_{3-\delta}$, which are used in SOFCs, are 4.34×10^{-2} S cm^{-1}, 8.75×10^{-2} S cm^{-1} and 1.72×10^{-1} S cm^{-1} at 1073 K [24], respectively. Taking into account that the total conductivity of the $GdSmZr_2O_7$ ceramic (5.30×10^{-3} S cm^{-1} at 1073 K) is slightly lower than those of conventional solid oxide electrolytes, the most likely applications of the $GdSmZr_2O_7$ ceramic in SOFCs are high-temperature solid electrolytes, or thick-film electrolytes, or as protective layers applied onto CeO_2- or $LaGaO_3$-based solid oxide electrolytes [24].

4. Conclusions

The $GdSmZr_2O_7$ ceramic sintered at 1673–1973 K for 10 h in air exhibits a single phase of the pyrochlore-type structure. The relative density of the $GdSmZr_2O_7$ ceramic rapidly increases with increasing sintering temperature. The total conductivity of the $GdSmZr_2O_7$ ceramic obeys the Arrhenius relation, and gradually increases with increasing temperature from 723 to 1173 K. The $GdSmZr_2O_7$ ceramic is an oxide-ion conductor in the oxygen partial pressure range of 1.0×10^{-4} to 1.0 atm at all test temperature levels. In the present work, the maximum value of the total conductivity for the $GdSmZr_2O_7$ ceramic is about 1.01×10^{-2} S cm^{-1} at 1173 K.

Acknowledgments

This work was financially supported by the National Natural Science Foundation of China (NSFC, Grant Nos. 50972030 and 51021002), the Fundamental Research Funds for the Central Universities (Grant Nos. HIT.BRET1.2010006 and HIT.NSRIF.201132), and the China Postdoctoral Science Foundation funded project (CPSF-Nos. 20100471029 and 201104419).

References

[1] L. Malavasi, C.A.J. Fisher, M.S. Islam, Chem. Soc. Rev. 39 (2010) 4370–4387.
[2] J. Malzbender, R.W. Steinbrech, L. Singheiser, Fuel Cells 9 (2009) 785–793.
[3] M.C. Tucker, J. Power Sources 195 (2010) 4570–4582.
[4] A.J. Jacobson, Chem. Mater. 22 (2010) 660–674.
[5] K.K. Hansen, M. Wandel, Y.L. Liu, M. Mogensen, Electrochim. Acta 55 (2010) 4606–4609.
[6] F. Smeacetto, M. Salvo, L.C. Ajitdoss, S. Perero, T. Moskalewicz, S. Boldrini, L. Doubova, M. Ferraris, Mater. Lett. 64 (2010) 2450–2453.
[7] A. Chen, G. Bourne, K. Siebein, R. DeHoff, E. Wachsman, K. Jones, J. Am. Ceram. Soc. 91 (2008) 2670–2675.
[8] J.A. Díaz-Guillén, A.F. Fuentes, M.R. Díaz-Guillén, J.M. Almanza, J. Santamaría, C. León, J. Power Sources 186 (2009) 349–352.
[9] M. Chen, Y.-L. Liu, A. Hagen, P.V. Hendriksen, F.W. Poulsen, Fuel Cells 9 (2009) 833–840.
[10] M.A. Subramanian, G. Aravamudan, G.V. Subba Rao, Prog. Solid State Chem. 15 (1983) 55–143.
[11] K. Shinozaki, M. Miyauchi, K. Kuroda, O. Sakurai, N. Mizutani, M. Kato, J. Am. Ceram. Soc. 62 (1979) 538–539.
[12] B.P. Mandal, A. Dutta, S.K. Deshpande, R.N. Basu, A.K. Tyagi, J. Mater. Res. 24 (2009) 2855–2862.
[13] Z.-G. Liu, J.-H. Ouyang, K.-N. Sun, X.-L. Xia, Electrochim. Acta 55 (2010) 8466–8470.
[14] Z.-G. Liu, J.-H. Ouyang, K.-N. Sun, Y. Zhou, Mater. Lett. 65 (2011) 385–387.
[15] Z.-G. Liu, J.-H. Ouyang, Y. Zhou, X.-L. Xia, J. Power Sources 185 (2008) 876–880.
[16] X. Sha, Z. Lü, X. Huang, J. Miao, Z. Liu, X. Xin, Y. Zhang, W. Su, J. Alloys Compd. 433 (2007) 274–278.
[17] B. Li, X. Wei, W. Pan, J. Power Sources 183 (2008) 498–505.
[18] Z.-G. Liu, J.-H. Ouyang, Y. Zhou, J. Mater. Sci. 43 (2008) 3596–3603.
[19] Z.H. Xu, S.M. He, L.M. He, R.D. Mu, G.H. Huang, X.Q. Cao, J. Alloys Compd. 509 (2011) 4273–4283.
[20] J.R. Macdonald, W.B. Johnson, in: E. Barsoukov, J.R. Macdonald (Eds.), Impedance Spectroscopy: Theory, Experiment and Applications, 2nd ed., John Wiley & Sons, Inc., New Jersey, 2005 (Chapter 1).
[21] Z.-G. Liu, J.-H. Ouyang, Y. Zhou, J. Xiang, Mater. Des. 32 (2011) 4201–4206.
[22] Z.-G. Liu, J.-H. Ouyang, K.-N. Sun, Fuel Cells 10 (2010) 1050–1056.
[23] J.B. Goodenough, Annu. Rev. Mater. Res. 33 (2003) 91–128.
[24] V.V. Kharton, F.M.B. Marques, A. Atkinson, Solid State Ionics 174 (2004) 135–149.